

# GUIDING THE WAY TO GAMMA-RAY SOURCES: X-RAY STUDIES OF SUPERNOVA REMNANTS

Patrick Slane

*Harvard-Smithsonian Center for Astrophysics*

*60 Garden Street*

*Cambridge, MA 02138*

*USA*

slane@cfa.harvard.edu

**Keywords:** Supernova Remnants,  $\gamma$ -ray sources

**Abstract** Supernova remnants have long been suggested as a class of potential counterparts to unidentified  $\gamma$ -ray sources. The mechanisms by which such  $\gamma$ -rays can arise may include emission from a pulsar associated with a remnant, or a variety of processes associated with energetic particles accelerated by the SNR shock. Imaging and spectral observations in the X-ray band can be used to identify properties of the remnants that lead to  $\gamma$ -ray emission, including the presence of pulsar-driven nebulae, nonthermal X-ray emission from the SNR shells, and the interaction of SNRs with dense surrounding material.

## 1. INTRODUCTION

Supernova remnants and their associated pulsars represent an energetic class of objects which is intimately connected to sources of  $\gamma$ -ray emission in our Galaxy. The connection between SNRs and the energetic cosmic rays that pervade the Galaxy has long been assumed, for example; shock acceleration by the SNR blast wave provides ample energy for the production of multi-TeV particles, and the presence of nearby material in dense clouds from which the remnant progenitors collapsed forms a natural target for pion production with subsequent  $\pi^0 \rightarrow 2\gamma$  decay. Nonthermal bremsstrahlung of electrons off ambient material, as well as inverse Compton scattering of electrons off ambient photons, can also lead to  $\gamma$ -ray production – and in many cases are the dominant mechanisms. SNRs are thus strong candidates for the emission of

$\gamma$ -rays. Recent observations have revealed remnants whose emission is dominated by nonthermal X-rays from these energetic particles, providing direct evidence of TeV electrons, and leading to the detection of two remnants as VHE  $\gamma$ -ray sources.

Gamma-ray studies to date have clearly identified pulsars as strong candidates for  $\gamma$ -ray emission (see Thompson – these proceedings), and SNRs hold another key in this regard. Recent X-ray observations (e.g. Slane et al. 1997; Harrus, Hughes, & Slane 1998; Harrus & Slane 1999) have revealed numerous new synchrotron nebulae in SNRs which, to the best of our understanding, must house magnetospherically active neutron stars. Studies with *Chandra* and XMM-Newton can realistically be expected to expand much of the ground breaking work done with ASCA in this regard, thus improving our ability to identify promising candidates for energetic  $\gamma$ -ray production. Here I review recent and ongoing observational X-ray work on composite remnants, SNR interactions with molecular clouds, and nonthermal emission from shell-type SNRs, and discuss how these might act as guides to sources of  $\gamma$ -ray emission.

## 2. GAMMA-RAYS FROM SNRS

The large positional uncertainties for EGRET sources, coupled with the extended nature of SNRs, make the clear identification of direct associations between the two populations a difficult task (Figure 1, left). Moreover, statistical assessment of the likelihood of a given association is complicated by the fact that the distribution of potential source candidates (e.g. SNRs, pulsars, OB associations) are not unrelated (Kaaret & Cottam 1996; Romero et al. 1999; Grenier, 2000). These results render positional coincidences unconvincing as the only evidence for an association between a particular SNR and EGRET source. X-ray observations probe several characteristics of SNRs and their environments which are directly related to  $\gamma$ -ray production, and are thus of considerable importance in establishing such associations. In addition, such observations can provide candidate SNRs for further, more sensitive  $\gamma$ -ray observations.

There are three primary means by which  $\gamma$ -rays might be associated with an SNR. Though only indirectly connected, the most prevalent is emission directly from an associated pulsar and/or a pulsar-driven synchrotron nebula. This is likely to be a viable mechanism for only somewhat young pulsars, and it is thus possible that the associated SNRs will still be detectable. A more direct mechanism is  $\pi^0$  decay through interaction of the SNR shell with dense material in a nearby molecular cloud. Finally, nonlinear shock acceleration at the SNR shell may result

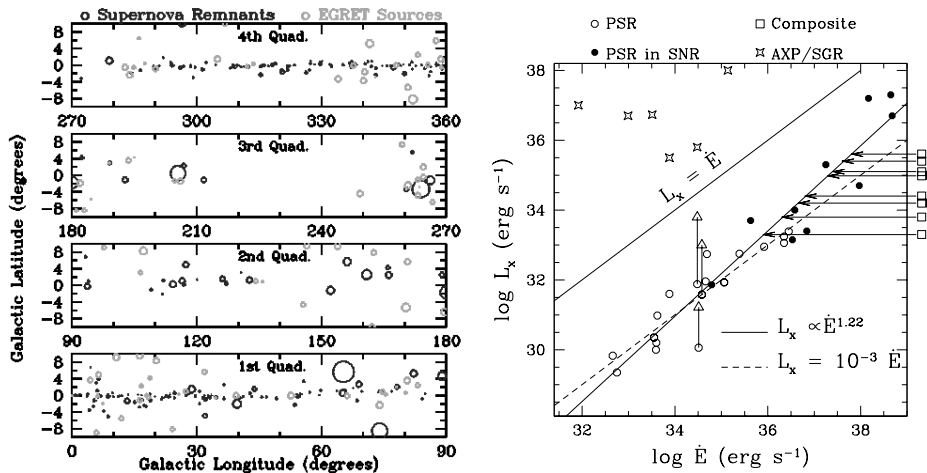


Figure 1 Left: Distribution of SNRs (black) and EGRET sources (grey) in the Galactic plane. Circles correspond approximately to SNR size or EGRET position error circles. Right:  $L_x$  vs.  $\dot{E}$  for pulsars and plerions. Triangles correspond to pulsars with identified cooling components, and the associated circles have this component subtracted. Luminosities include emission from associated synchrotron nebula where known. For composite SNRs whose pulsars are not detected,  $L_x$  is plotted along the right axis. Arrows indicate where these objects would reside on the  $L_x$  vs.  $\dot{E}$  diagram. Note the good agreement between these values and those for young pulsars in SNRs (filled circles).

in inverse Compton and/or nonthermal bremsstrahlung radiation from energetic electrons accelerated by the SNR. Each of these scenarios can be associated with particular characteristics of the SNR X-ray emission. I discuss these cases briefly, and present possible examples of each.

## 2.1. PULSARS AND SYNCHROTRON NEBULAE

Since the majority of SNe result from massive star collapse, and most such collapses are expected to form neutron stars (NSs), it is reasonable to expect that young NSs should be associated with most young SNRs. If all young NSs are rapidly rotating, magnetospherically active pulsars, the corollary would then suggest that these SNRs are likely to be sources of energetic  $\gamma$ -ray emission since pulsars are a well-established class of  $\gamma$ -ray sources. In practice, however, there are numerous examples of young SNRs for which no associated NS is observed. Moreover, recent observations have revealed compact X-ray sources, apparently associated with SNRs, whose properties differ considerably from those

of Crab-like pulsars (see Caraveo, Bignami, & Trümper 1996; Kaspi 2000). These include the Anomalous X-ray Pulsars (AXPs) such as 1E 2259+586 in the remnant CTB 109, the radio-quiet neutron stars such as PKS 1209–51/52 in Puppis A (Zavlin, Trümper, & Pavlov 1999), and the point source in Cas A, whose properties are unlike any of the above (Pavlov et al. 2000). In cases where an X-ray emitting synchrotron nebula (or “plerion”) is observed, however, we infer the presence of a young pulsar powering the nebula. Remnants displaying such a component are thus good candidates for  $\gamma$ -ray emission.

Empirically, it is found that there exists a relationship between  $\dot{E}$ , the pulsar energy loss rate, and  $L_x$ , the total X-ray luminosity from the pulsar (not including any cooling component) and its associated synchrotron nebula (Seward & Wang 1988; Becker & Trümper 1997). Thus, even in the absence of direct detection of a pulsar, its properties can be inferred from the nonthermal X-ray spectrum of the plerion. This is illustrated in Figure 1 (right) where I have plotted values for known pulsars. Synchrotron nebulae in composite SNRs for which no pulsar has yet been identified are shown as well. It is important to note, however, that variations in the  $L_x$  vs.  $\dot{E}$  relation are large. This is due, at least in part, to the variety of conditions inherent to the systems used to establish the relation (bow shock nebulae, plerions interacting with supernova ejecta, etc.). This has been addressed in recent work by Chevalier (2000), who has developed a one-zone model for the X-ray properties of pulsar nebulae which accounts for differences in the relative efficiency with which  $L_x$  is produced, based on the cooling regime in which the electrons find themselves after passing through the wind termination shock.

**G21.5–0.9.** Although we infer the presence of an active, young NS with any X-ray synchrotron nebula, it is by no means the case that pulsars have been identified for each. G21.5–0.9, for example, is a well-defined plerion for which radio observations show no direct evidence of a compact central source. *Chandra* observations (Slane et al. 2000) reveal a compact source at the center of the nebula, but the high resolution images clearly demonstrate that the source is slightly extended. Using the radio spectrum to estimate the magnetic field strength of the nebula under the assumption of equipartition between the field and the particles, and requiring that this associated magnetic pressure act to confine a pulsar wind driven by the spin-down power,  $\dot{E} = 3.5 \times 10^{37} d_5^{1.6} \text{ erg cm}^{-2} \text{ s}^{-1}$ , of a central pulsar (using the empirical  $\dot{E}$  vs.  $L_x$  relationship, with  $d_5$  as the distance in units of 5 kpc) indicates that the extended size of the central emission is consistent with

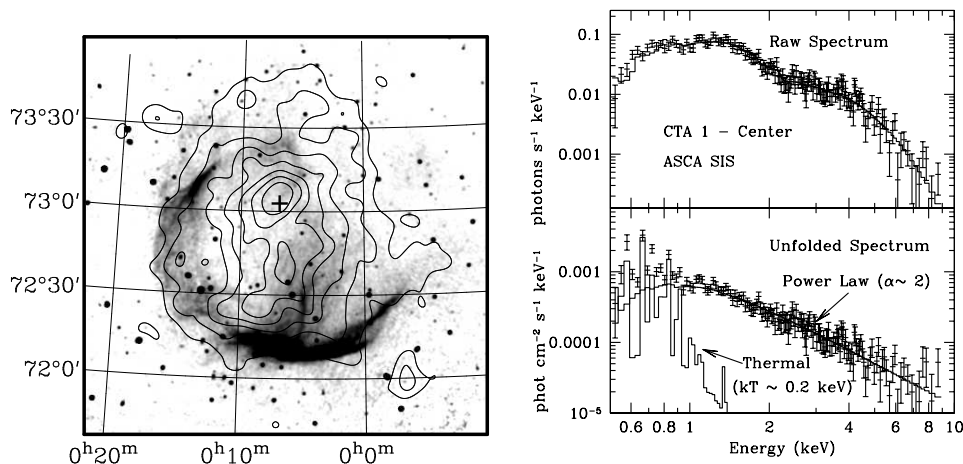


Figure 2 Left: Continuum image of CTA 1 at 1420 MHz with X-ray contours from the ROSAT PSPC. (Radio image kindly provided by T. Landecker.) Note the incomplete shell-like radio morphology contrasted with the centrally bright X-ray morphology. The position of the faint point source J000702+7302.9 is indicated with a cross. Right: ASCA data extracted from SIS chip centered on central region of CTA 1. Upper: Raw spectrum with best-fit power-law plus thermal model. Lower: Unfolded spectrum and model components.

the radius of the stand-off shock where the wind is confined. A smaller  $\dot{E}$  is predicted by the model of Chevalier (2000), resulting in a smaller estimated shock radius, but one still in rough agreement with the observations. As the particle wind traverses the standoff shock, the nebular structure changes from a particle-dominated to a magnetic-dominated flow (Kennel & Coroniti 1984). The finite lifetime of the synchrotron emitting electrons results in a steepening of the spectrum with radius, an effect clearly observed in G21.5–0.9 (Slane et al. 2000). Thus, the X-ray observations indicate the presence of an energetic pulsar in G21.5–0.9. The inferred value of  $\dot{E}/d^2$  (a rough indicator of the expected  $\gamma$ -ray flux) is larger than that for many of the known  $\gamma$ -ray pulsars (or for only several, using the value estimated by Chevalier) suggesting that sensitive  $\gamma$ -ray observations of this source may be of interest.

**CTA1 and 2EG J0008+7303.** Another example of the pulsar-perlerion connection of particular interest in the context of  $\gamma$ -ray sources in that of CTA 1. In the radio band, CTA 1 (G119.5+10.3) consists of an incomplete shell (Figure 2) with faint emission extending to the northwest in what may be a breakout region (Pineault et al. 1997). The X-ray morphology is centrally brightened with emission bounded by the radio

shell in the south and west, and with faint emission extending into the breakout region. ROSAT PSPC observations indicate a two-component spectrum for which the hard component dominates in the central regions but becomes weaker in the outer regions of the remnant (Seward, Schmidt, & Slane 1995). A faint X-ray source (J000702+7302.9) is found at the peak of the central X-ray emission (Figure 2).

ASCA observations of CTA 1 (Slane et al. 1997) reveal a nonthermal central spectrum clearly indicating the composite nature of this remnant (Figure 2). This is bolstered by the presence of the EGRET source 2EG J0008+7303 whose error circle includes the position of the faint X-ray source (Brazier et al. 1997) and whose spectrum, when extrapolated to the soft X-ray band, is consistent with that measured for J000702+7302.9 (although the latter fact is not necessarily expected from emission models).

The nonthermal X-ray luminosity is  $5.6 \times 10^{33} D_{1.4}^2 \text{ erg s}^{-1}$  leading to an inferred pulsar energy loss rate of  $\dot{E} = 1.7 \times 10^{36} D_{1.4}^{1.4} \text{ erg s}^{-1}$ . If correct, the value of  $\dot{E}/d^2$  is exceeded by only 4 pulsars, all of which (along with 4-5 with smaller values) are known  $\gamma$ -ray sources. The X-ray measurements thus strongly indicate that 2EG J0008+7303 is associated with the X-ray source and synchrotron nebula in CTA 1. Modeling of outer gap  $\gamma$ -ray production (Zhang & Cheng 1998) indicates that a  $\gamma$ -ray pulsar scenario for this source is indeed feasible. Deeper X-ray observations of this source are currently underway with XMM-Newton.

#### **Other Plerionic Candidates.**

In addition to the Crab and Vela pulsars, both associated with synchrotron nebulae, and both well-known  $\gamma$ -ray pulsars, there are several EGRET sources for which X-ray observations suggest a pulsar (or pulsar-driven nebula) counterpart. Halpern et al. (2001) use X-ray, radio, and optical data to show that 3EG J2227+6122 may be associated with a pulsar-powered source. An incomplete circular shell within the EGRET error circle is seen in VLA sky survey data, and ASCA data from this region reveals emission well-described by a power law. The radio image resembles a bow-shock nebula or wind-blown bubble, and the X-ray properties are consistent with such an interpretation.

ASCA observations of the region around 2EG J1418–6049 (Roberts and Romani 1998) also suggest a pulsar wind nebula interpretation for this source. The X-ray image reveals an extended nonthermal object whose properties are consistent with being a nebula energized by a pulsar with a characteristic age of  $\sim 10^{4.5}$  yr.

Extended nonthermal X-ray emission is also observed within the error circle of 2EG J1811–2339 (Oka et al. 1999). These authors suggest

that the source may be a synchrotron nebula associated with a currently unknown pulsar, and that the nebula may be interacting with a dense cloud of material seen in CO observations. In this case, the  $\gamma$ -ray emission may only be indirectly associated with the pulsar, which may act as a source of electrons that undergo shock acceleration at the cloud interaction site. Several other SNRs with nearby pulsars have been suggested as counterparts for EGRET sources (e.g. W44 and W28), but it appears that the  $\gamma$ -ray emission from these sources is also associated with the remnants and not the pulsars. Such interaction processes are discussed in more detail below.

## 2.2. PARTICLE ACCELERATION BY SNR SHOCKS

Beyond the early  $\gamma$ -ray emission fueled by the radioactive decay of unstable isotopes formed in supernovae, the mechanical energy released in the explosions can be transformed into  $\gamma$ -ray emission over a longer period of time. As the blast wave from the explosion expands, material from the surrounding circumstellar material (CSM) and ISM is swept up into a shell of hot gas. For an ideal  $\gamma = 5/3$  gas, the shock jump conditions yield an increase in density by a factor of 4 and a postshock temperature

$$T = \frac{3\mu m}{16k} V_s^2$$

where  $V_s$  is the shock speed,  $m$  is the proton mass, and  $\mu$  is the mean molecular weight of the gas ( $\mu \approx 0.6$ ). This shock-heated gas yields the familiar X-ray emission, characterized by a thermal bremsstrahlung spectrum accompanied by strong emission lines.

As increasing amounts of material are swept up by the blast wave, the shock is decelerated and the ejecta from the explosion encounter the dense shell. A reverse-shock is generated, heating the ejecta. At early times, then, the X-ray spectrum is dominated by emission from the ejecta. As the amount of swept-up material increases, the spectrum becomes dominated by emission from material with ISM abundances.

In addition to thermal heating of the swept-up gas, some fraction of the shock energy density goes into nonthermal production of relativistic particles through diffuse shock acceleration. Particle acceleration by SNR shocks has, of course, been suggested for decades as a process by which cosmic rays are produced. Radio observations of SNRs provide ample evidence of electrons with GeV energies through synchrotron radiation in the compressed magnetic field at the remnant shell. At higher particle energies,  $\gamma$ -ray production may result from nonthermal bremsstrahlung of electrons colliding with ambient gas, from inverse

Compton scattering of ambient photons, and from the decay of neutral pions created by the collision of energetic protons. If the relativistic particle component of the energy density becomes comparable to that of the thermal component, the shock acceleration process can become highly nonlinear. The gas becomes more compressible, which results in a higher density and enhanced acceleration. This process has been considered in detail by Baring et al. (1999) who present a model for the radio to  $\gamma$ -ray emission. The relative contributions from the different  $\gamma$ -ray production mechanisms depend highly on ambient conditions, and X-ray studies of these SNRs reveal these conditions and can provide spectral measurements which highly constrain the models. Here I summarize the X-ray properties of several SNRs which may be associated with  $\gamma$ -ray emission, in an effort to illustrate these ideas.

### 2.3. PION DECAY AND MOLECULAR CLOUD INTERACTIONS

If the blast wave of an SNR is capable of accelerating protons (or other ions) to sufficiently high energies, then the interaction of these particles with ambient material can result in the production of neutral pions which subsequently decay into  $\gamma$ -rays. The  $\gamma$ -ray flux for such a process was calculated by Drury, Aharonian, & Völk (1994). For a power-law particle spectrum with spectral index  $\alpha \sim 2.1 - 2.3$ , the flux is

$$F_{\gamma}(\geq E_{\text{TeV}}) \approx 5 \times 10^{-11} \epsilon E_{51} d_{\text{kpc}}^{-2} n E_{\text{TeV}}^{-\alpha+1} \text{ cm}^{-2} \text{ s}^{-1}$$

where  $\epsilon$  is the fraction of the blast wave energy ( $E_{51}$ , in units of  $10^{51}$  erg) converted into cosmic ray energy,  $d_{\text{kpc}}$  is the SNR distance in kpc,  $n$  is the number density of the ambient medium, and  $E_{\text{TeV}}$  is the  $\gamma$ -ray energy in TeV. The leading numerical factor actually depends on  $\alpha$ ; I have taken an average value which is accurate to within a factor of two or so over the stated range for  $\alpha$ . This spectrum is plotted in Figure 3 (left) for two values of  $\epsilon$ , the larger of which is probably an overestimate of what can typically be extracted from this process. Here I have assumed  $n = 1 \text{ cm}^{-3}$ , and  $E_{51} = d_{\text{kpc}} = 1$ . Also shown are approximate sensitivities for EGRET, GLAST, and VERITAS. Note that, for typical SNR parameters, the predicted flux is near or below the EGRET sensitivity, although above the sensitivity limits for GLAST or VERITAS.

For cases in which the SNR is encountering dense material (i.e.  $n \gg 1$ ), such as in an interaction with a nearby molecular cloud, the  $\gamma$ -ray flux can be enhanced considerably. In a model for the evolution of SNRs in molecular clouds, Chevalier (1999) argues that the  $\gamma$ -ray emission

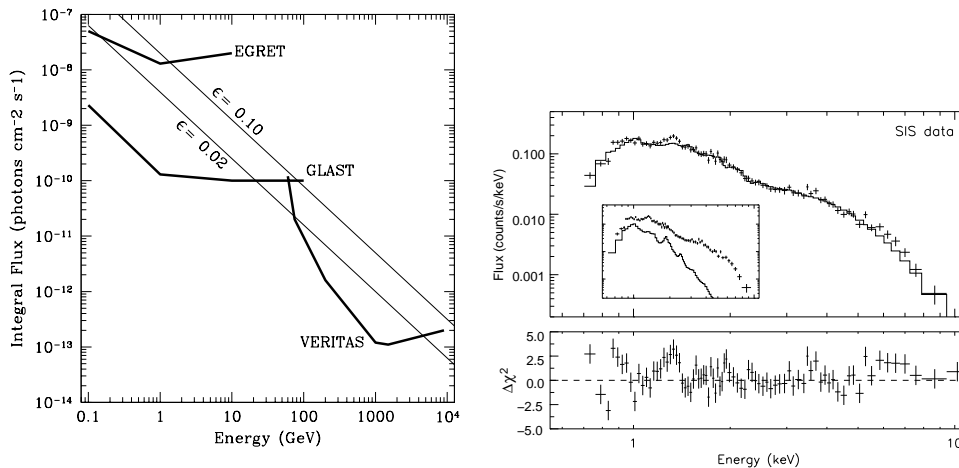


Figure 3 Left: Model pion-decay  $\gamma$ -ray flux from SNRs (see text). Also shown are detection sensitivities for EGRET, GLAST, and VERITAS. Right: X-ray spectrum from MSH 11-62 showing clear evidence of a synchrotron component.

results from the radiative shell of the remnant where some fraction of the energy density in the postshock region goes into relativistic particles. Bremsstrahlung interactions in the dense shell yield the high energy emission, and synchrotron radiation from this population, in the compressed magnetic field, can simultaneously produce the observed radio emission. Because massive stars live their lives quickly, they expire nearby the molecular clouds from which they formed; the ensuing supernova explosion can thus lead to direct interaction with the molecular clouds. Such SNR/cloud interactions are most clearly identified through OH maser emission (e.g. Frail et al. 1996), although CO mapping also provides an important means of tracing the molecular gas around SNRs.

The X-ray properties of SNRs can also provide an indication of such interactions. SNR/cloud interactions can result in a significant brightening of the interaction region due to the increase in density. For example, molecular clouds may be associated with the so-called “mixed morphology” (MM) class of remnants (Rho & Petre 1998). These SNRs are characterized by a center-filled X-ray morphology, as might be expected for a shell-type remnant whose central region contains a pulsar-powered nebula, but in this case the emission is thermal in nature, and the radial temperature profile is relatively flat. Several models have been put forth to explain the brightness and temperature profiles for these SNRs. The cloud evaporation model derived by White and Long (1991) has been applied to the emission from W44 (Harrus et al. 1996), G272.2–3.2

(Harrus et al. 2001), MSH 11–61A (Slane et al. 2001), and others. In this model the SNR evolves in a two-phase interstellar medium (ISM) consisting of cool, dense clouds and a low density intercloud medium. The SNR shock sweeps past the clouds quickly, leaving them to slowly evaporate in the hot SNR interior, thus contributing X-ray emitting material to the central regions. Harrus et al. (1996) also considered a model for W44 in which the remnant had entered the radiative phase, thus leaving the shell too cool to radiate significantly in X-rays, but allowing the emission from the hotter interior to persist. W44 is known to be interacting with an adjacent molecular cloud, which is consistent with deceleration of the shock and evolution into the radiative phase. Shelton et al. (1999) extended this picture significantly by including the effects of thermal conduction on smoothing out the temperature and density profile of the X-ray emission material. Slane et al. (2001) applied both models to emission from MSH 11–61A.

Other SNRs which fit into this MM class include W28 (Long et al. 1991) and IC 443 (Petre et al. 1988, Asaoka & Aschenbach 1994), two remnants which (along with W44) have been suggested as counterparts to EGRET sources; each is known to be interacting with a molecular cloud. Romero et al. (1999) have compiled a list of SNRs with positional coincidences with EGRET sources, and at least one-third of these show some indication of the presence of molecular clouds. As noted above, these positional coincidences are far from convincing evidence that each of these SNRs are associated with  $\gamma$ -ray sources, but the presence of dense material provides some supporting evidence.

**MSH 11–61A and 3EG J1101–6103.** The unidentified EGRET source 3EG J1101–6103 provides an interesting case for which each of the topics above deserves consideration. Early catalogs associated this source with MSH 11–62. X-ray observations (Harrus, Hughes, & Slane 1998) reveal the remnant to be composite in nature, with a two-component spectrum (Figure 3, right) consisting of a central nonthermal component and an extended thermal component. As noted above, the presence of a synchrotron nebula is indicative of a young pulsar, making the association a reasonable one. An improved position for the EGRET source revealed that MSH 11–62 falls outside the error circle, however (Figure 4, left).

Kaspi et al. (1997) identified a young pulsar PSR J1105–6107 which lies within the error circle, and suggested an association between the pulsar and the nearby remnant MSH 11–61A (Figure 4). The value of  $\dot{E}/d^2$  for this pulsar is quite low for a  $\gamma$ -ray source, however, though higher than that for PSR B1055–52 which is detected by EGRET. Moreover,

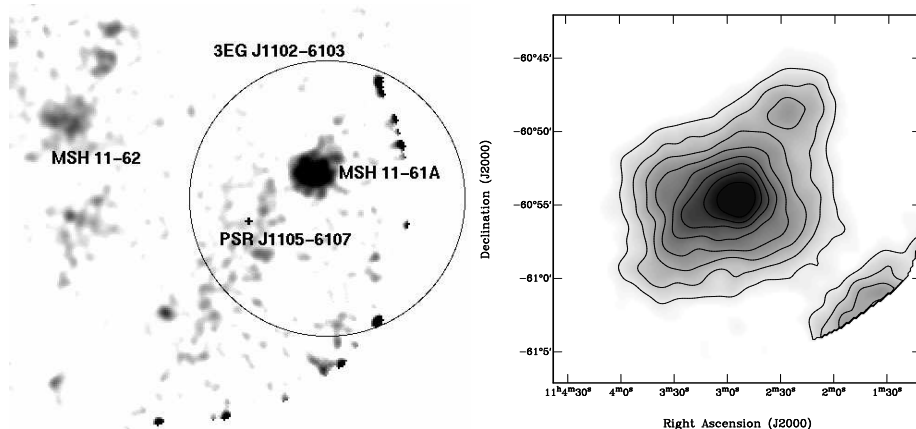


*Figure 4* Left: X-ray emission from region surrounding 3EG J1102–6103. Right: ASCA GIS image of MSH 11–61A. Emission at the southwest edge of the field is associated with an off-axis source just outside the primary telescope field of view.

X-ray studies indicate that an association between the pulsar and the SNR is unlikely (Slane et al. 2001).

It is of interest that MSH 11–61A lies along the line of sight to a dense molecular cloud whose distance ( $\sim 7$  kpc), from CO measurements appears consistent with that estimated for the remnant. Petruk (2000) has suggested that the mixed-morphology nature of this remnant (and others) is the result of enhanced emission from a cloud interaction directly along the line of sight. Further, this same picture is used to estimate the  $\pi^0$ -decay  $\gamma$ -ray luminosity. For a cloud density of  $\sim 40$   $\text{cm}^{-2}$ , the predicted flux (assuming  $\epsilon = 0.1$ ) matches that of 3EG J1101–6103. Efforts to model the observed X-ray temperature and brightness profiles under this scenario are underway. An important point, however, is that more complete modeling of the particle acceleration process in shock-cloud interactions indicates that emission from pion decay falls considerably below that from bremsstrahlung (Gaisser et al. 1998, Bykov et al. 2000).

## 2.4. NONTHERMAL X-RAY EMISSION FROM SNRS

While the shock-heated ejecta and CSM/ISM components of shell-type SNRs produce line-dominated X-ray spectra, as described above, a growing number of remnants also reveal evidence of hard, nonthermal X-ray emission components, apparently associated with high energy electrons accelerated by the SNR shock. In three cases – SN 1006 (Koyama et al. 1995), G347.3–0.5 (Koyama et al. 1997; Slane et al. 1999), and

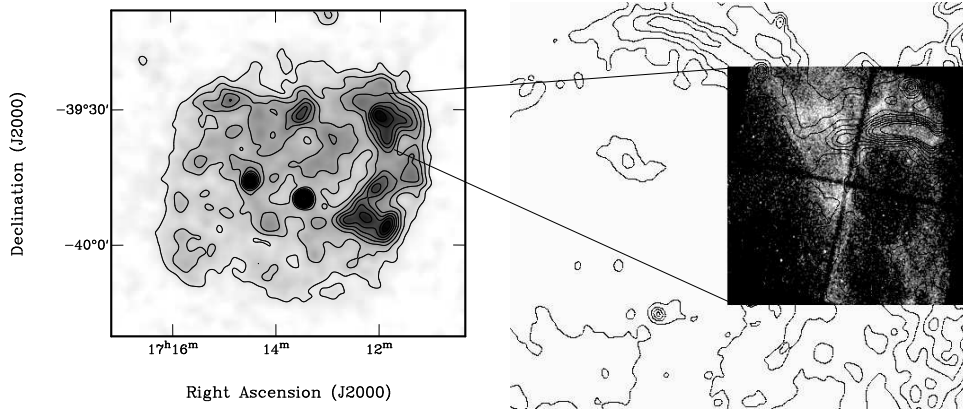
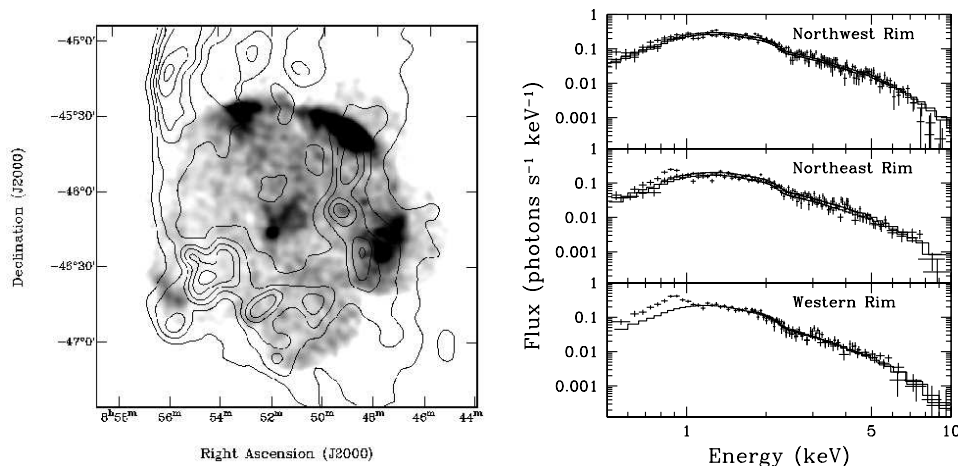


Figure 5 Left: ROSAT PSPC image of G347.3–0.5. Right: *Chandra* image of northwest rim, with radio contours from ATCA.

G266.2–1.2 (Slane et al. 2001) – the nonthermal emission components completely dominate the thermal components, and the X-ray spectra from the shells are featureless.

Although the radio emission from SNRs provides direct evidence of GeV electrons, it is the recent detections of nonthermal X-rays from shell-type SNRs that provide direct evidence of particles accelerated to energies as high as 10 – 100 TeV, approaching the knee in the cosmic ray spectrum. Models for nonlinear shock acceleration (e.g. Ellison, Berezhko, & Baring 2000) predict a strong correlation between the radio, X-ray, and  $\gamma$ -ray flux that allow parameters of the acceleration process to be derived. It is thus of considerable interest to localize the regions of nonthermal X-ray emission, and to investigate the broad-band spectra (particularly in radio, X-rays, and  $\gamma$ -rays) from these regions.

In Figure 5, I present a preliminary *Chandra* image of the X-ray emission from the NW limb of G347.3–0.5, whose shell emission is nonthermal. Overlaid are radio contours from the Australia Telescope Compact Array (ATCA), showing good general correspondence between the components. This region of the SNR has also been detected as a source of  $\sim$ TeV  $\gamma$ -rays (Muraishi et al. 2000). Preliminary modeling suggests a self-consistent picture in which the X-ray and radio flux is synchrotron radiation from the accelerated electrons, while the  $\gamma$ -ray flux represents inverse-Compton scattering of energetic electrons off of the microwave background (Ellison, Slane, & Gaensler – in preparation). The predicted GeV flux falls below the EGRET threshold, but should be detectable with GLAST. Such measurements, along with more sensitive



*Figure 6* Left: ASCA GIS image of G266.2-1.2 ( $E = 0.7 - 10$  keV). The image consists of a mosaic of 7 individual fields. Contours represent the outline of the Vela SNR as seen in ROSAT survey data with the PSPC. Right: ASCA spectra from both GIS detectors for regions of G266.2-1.2. The featureless spectrum is well described by a power law. Excess flux at low energies is presumably associated with soft thermal emission from the Vela SNR.

X-ray observations, will provide significant information for constraining the parameters of these models.

G266.2-1.2 was discovered by Aschenbach (1998) using data from the ROSAT All-Sky Survey. Situated along the line of sight to the Vela SNR, the X-ray emission stands out above the soft thermal emission from Vela only at energies above  $\sim 1$  keV. ASCA observations show that the emission from G266.2-1.2 is nonthermal (Slane et al. 2001), providing another example of a shell-type SNR for which the X-ray emission is dominated by such processes. CO data (May et al. 1988) reveal a concentration of giant molecular clouds – the Vela Molecular Ridge – at a distance of  $\sim 1 - 2$  kpc in the direction of Vela. The X-ray observations of G266.2-1.2 indicated a column density consistent with the remnant being located near, but probably not beyond, this molecular material. More sensitive X-ray measurements are required to investigate the shock structure and spectrum, for comparison with nonlinear shock models. Observations at TeV energies are of considerable interest, particularly given that SN 1006 and G347.3-0.5 have both been detected at such energies. Given the relatively small distance to this remnant, it would appear to be an excellent candidate for future observations with GLAST as well.

### 3. SUMMARY

Several mechanisms exist by which SNRs may be associated with the emission of energetic  $\gamma$ -rays. X-ray observations provide powerful clues by which the properties of these mechanisms can be revealed. Through the identification of pulsar-driven nebulae, nonthermal emission from particles accelerated at the SNR shell, or sites of interactions with dense clouds, X-ray studies of SNRs are helping to resolve at least some of the questions centered on the nature of unidentified EGRET sources. The prospects for continued success in this area are extremely encouraging. The capabilities of current X-ray observatories, coupled with upcoming  $\gamma$ -ray missions (both space and ground based), promise not only to help identify the counterparts to these sources of  $\gamma$ -rays, but also to provide new and powerful constraints on developing models for such emission.

### Acknowledgments

The author wishes to thank Don Ellison and Glenn Allen for helpful discussions on nonthermal emission from SNRs. This work was supported in part by NASA through contract NAS8-39073 and grants NAG5-9106 and NAG5-9281.

### References

- Asaoka, I. & Aschenbach, B. 1994, *A&A*, **284**, 573  
 Aschenbach, B. 1998 *Nature*, **396**, 141  
 Baring, M. G., Ellison, D. C., Reynolds, S. P., Grenier, I. A., & Goret, P. 1999, *ApJ*, **513**, 311  
 Becker, W. & Trümper, J. 1997, *A&A*, **326**, 682  
 Brazier, K.T.S., Reimer, O., Kanbach, G., & Carraminana, A. 1997, *MNRAS*, **295**, 819  
 Bykov, A. M., Chevalier, R. A., Ellison, D. C., & Uvarov, Yu. A. 2000, *ApJ*, **538**, 203  
 Caraveo, P. A., Bignami, G. F., & Trümper, J. 1996, *A&A Rev.*, **7**, 209  
 Chevalier, R. A. 1999, *ApJ*, **511**, 798  
 Chevalier, R. A. 2000, *ApJ*, **539**, L45  
 Drury, L. O'C, Aharonian, F. A., & Völk, H. J. 1994, *A&A*, **297**, 959  
 Ellison, D. C., Berezhko, El G., & Baring, M. G. 2000, *ApJ*, **540**, 292  
 Frail, D. A., Goss, W. M., Reynoso, E. M., Giacani, E. B., Green, A. J., Otrupcek, R. 1996, *AJ*, **111**, 1651  
 Gaisser, T. K., Protheroe, R. J., & Stanev, T. 1998 *ApJ*, **492**, 21  
 Grenier, I. A. 2001, *A&A* **364**, L93  
 Halpern, J. P., Gotthelf, E. V., Leightly, K. M., & Helfand, D. J. 2001, *ApJ*, in press  
 Harrus, I. M., Hughes, J. P., & Helfand, D. J. 1996, *ApJ*, **464**, L161

- Harrus, I. M., Hughes, J. P., & Slane, P. O. 1998, *ApJ*, **499**, 273
- Harrus, I. M. & Slane, P. O. 1999, *ApJ*, **516**, 811
- Harrus, I. M., Slane, P. O., Smith, R. K., & Hughes, J. P. 2001, *ApJ* – in press
- Kaaret, P. & Cottam, J. 1996, *ApJ*, **462**, L35
- Kaspi, V. M., Bailes, M., Manchester, R. N., Stappers, B. W., Sandhu, J. S., Navarro, J., & D’Amico, N. 1997, *ApJ*, **485**, 820
- Kaspi, V. M. 2000, in ASP Conf. Ser. 202, Pulsar Astronomy 2000 and Beyond, ed. M. Kramer, N. Wex, & R. Wielebinski (San Francisco: ASP), 485
- Kennel, C. F. & Coroniti, F. V. 1984, *ApJ*, **283**, 710
- Koyama, K. et al. 1995 *Nature* **378**, 255
- Koyama, K. et al. 1997, *PASJ*, **49**, L7
- Long, K. S., Blair, William P., Matsui, Yutaka, White, Richard L. 1991, *ApJ*, **373**, 567
- May, J., Murphy, D. C., & Thaddeus, P. 1988, *A&ASS* **73**, 51
- Muraishi, H. et al. 2000, *A&A*, **354**, L57
- Oka, T., Kawai, N., Naito, T., Horiuchi, T., Namiki, M., Saito, Y., Romani, R. W., & Kifune, T. 1999, *ApJ*, **526**, 764
- Pavlov, G. G., Zavlin, V. E., Aschenbach, B., Trümper, J., & Sanwal, D. 2000, *ApJ*, **531**, L53
- Petre, R., Szymkowiak, A. E., Seward, F. D., Willingale, R. 1988, *ApJ*, **335**, 215
- Petruk, O, 2001, in Proceedings of NATO Advanced Study Institute “Astrophysical Sources of High Energy Particles & Radiation”, (Erice, Italy, 11-21 November 2000, eds. J. P. Wefel, M. M. Shapiro, & T. Stanev.
- Pineault, S., Landecker, T.L., Swerdlyk, C.M., & Reich, W. 1997, *A&A*, **324**, 1152
- Rho, J.-H. & Petre, R. 1998, *ApJ*, **503**, L167
- Roberts, M. S. E. & Romani, R. W. 1998, *ApJ*, **496**, 827
- Romero, G. E., Benaglia, P., & Torres, D. F. 1999, *A&A*, **348**, 868
- Seward, F.D., Schmidt, B., and Slane, P. 1995, *ApJ*, **453**, 284
- Seward, F.D. & Wang, Z.-R. 1988, *ApJ*, **332**, 199
- Shelton, R. L., Cox, Donald P., Maciejewski, Witold, Smith, Randall K., Plewa, Tomasz, Pawl, Andrew, & Rzyczka, Michal 1999, *ApJ*, **524**, 192
- Slane, P., Seward, F.D., Bandiera, R., Torii, K., & Tsunemi, H. 1997, *ApJ*, **481**, 225
- Slane, P. et al. 1999, *ApJ*, **525**, 357
- Slane, P., Chen, Y., Schulz, N. S., Seward, F. D., Hughes, J. P., & Gaensler, B. M. 2000, *ApJ*, **533**, L29

- Slane, P. et al. 2001, *ApJ* - accepted (see astro-ph/0010510)
- Slane, P., Hughes, J. P., Smith, R. K., & Petre, R. 2001, *ApJ* - submitted
- White, R. L. & Long, K. S. 1991, *ApJ*, **373**, 543
- Zavlin, V. E., Trümper, J., & Pavlov, G. G. 1999, *ApJ*, **525**, 959
- Zhang, L. & Cheng, K. S. 1998, *A&A*, **335**, 234